

DELFT UNIVERSITY OF TECHNOLOGY

REPORT 11-04

ON THE USE OF RIGID BODY MODES IN THE DEFLATED
PRECONDITIONED CONJUGATE GRADIENT METHOD.

T.B. JÖNSTHÖVEL, M.B. VAN GIJZEN, C. VUIK, A. SCARPAS

ISSN 1389-6520

Reports of the Department of Applied Mathematical Analysis

Delft 2011

Copyright © 2011 by Department of Applied Mathematical Analysis, Delft,
The Netherlands.

No part of the Journal may be reproduced, stored in a retrieval system, or transmitted, in any form or by any means, electronic, mechanical, photocopying, recording, or otherwise, without the prior written permission from Department of Applied Mathematical Analysis, Delft University of Technology, The Netherlands.

ON THE USE OF RIGID BODY MODES IN THE DEFLATED PRECONDITIONED CONJUGATE GRADIENT METHOD

T.B. JÖNSTHÖVEL[†], M.B. VAN GIJZEN, C. VUIK[‡], AND A. SCARPAS[†]

ABSTRACT. Large discontinuities in material properties, such as encountered in composite materials, lead to ill-conditioned systems of linear equations. These discontinuities give rise to small eigenvalues that may negatively affect the convergence of iterative solution methods such as the Preconditioned Conjugate Gradient (PCG) method. This paper considers the Deflated Preconditioned Conjugate Gradient (DPCG) method for solving such systems. Our deflation technique uses as the deflation space the rigid body modes of sets of elements with homogeneous material properties. We show that in the deflated spectrum the small eigenvalues are mapped to zero and no longer negatively affect the convergence. We justify our approach through mathematical analysis and we show with numerical experiments on both academic and realistic test problems that the convergence of our DPCG method is independent of discontinuities in the material properties.

1. INTRODUCTION

Finite element computations are indispensable for the simulation of material behavior. Recent developments in visualization and meshing software give rise to high-quality but very large meshes. As a result, large systems with millions of degrees of freedom need to be solved. In our application, the finite element stiffness matrix is symmetric, positive definite and therefore the Preconditioned Conjugate Gradient (PCG) method is the method of choice. The PCG method is also well suited for parallel implementations which are needed in practical applications.

Many finite element computations involve simulation of *inhomogenous* materials. The difference in properties of materials lead to large jumps in the entries of the stiffness matrix. We have shown in [8] that these jumps slow down the convergence of the PCG method. By decoupling those regions with a deflation technique a more robust PCG method can be constructed: the Deflated Preconditioned Conjugate Gradient (DPCG) method.

The deflation based preconditioners have successfully been applied within the field of computational fluid dynamics, with excellent results on problems with discontinuous jumps in coefficients [16], [5],[15]. We extend the technique of subdomain deflation, introduced in [13], to rigid body modes deflation to remove the effect of the rigid body modes from the linear system. The concept of using rigid body modes to speed up computations has been widely used in algebraic multigrid methods [18], [7] and the FETI framework [11], [10]. However, in this paper we present a new deflation strategy of using rigid body modes based on the underlying geometry and the physical properties

2000 *Mathematics Subject Classification.* 65F10, 65F08, 65Z05.

Key words and phrases. deflation, preconditioners, conjugate gradients, rigid body modes, CT scan, structural mechanics.

[†]Delft University of Technology, Faculty of Civil Engineering, Department of Structural Mechanics, 2628CN Delft, the Netherlands (t.b.jonsthovel@tudelft.nl, a.scarpas@tudelft.nl).

[‡]Delft University of Technology, Faculty of Information Technology and Systems, Department of Applied Mathematical Analysis, 2628CN Delft, the Netherlands (m.b.vangijzen@tudelft.nl, c.vuik@tudelft.nl).

of the problem. Moreover, we note that as far as we know this is the first successful application of deflation based preconditioning applied to *coupled* systems of partial differential equations.

In [8] we showed there is a correlation between the number of rigid body modes of sub-bodies of materials contained within the FE mesh and the number of small eigenvalues of the stiffness matrix. We used rigid body modes combined with existing deflation techniques to remove those small eigenvalues from the spectrum of the stiffness matrix. We introduced the DPCG method that uses deflation vectors that contain the rigid body modes of sets of elements with similar properties. In this paper we will show how to choose these sets of elements and provide a mathematical justification of this choice. We will derive a cheap and general applicable method to compute those rigid body modes. Finally, we will present numerical experiments on composite materials to validate our results.

2. PROBLEM DEFINITION: COMPOSITE MATERIALS

Until recently, because of the extremely long execution time, memory and storage space demands, the majority of FE simulations of composite materials were performed by means of homogenization techniques [4]. Unfortunately these techniques do not provide an understanding of the actual interaction between the components of the material. Nevertheless, it is known that component interaction is the most critical factor in determining the overall mechanical response of the composite material.

In this paper, we consider asphalt concrete as an example of a composite material. It consists of a mixture of bitumen, aggregates and air voids. Obviously the difference between the stiffness of bitumen and the aggregates is significant, especially at high temperatures.

We obtain accurate finite element meshes of the asphalt concrete materials by means of Computed Tomography (CT) X-ray scans and additional, specialized software tools like Simpleware ScanFE [14].

We use the computational framework described in [4] to simulate the response of a composite material that is subjected to external forces by means of small load steps. By using the FE method we obtain the corresponding stiffness matrix. Solving linear system (1),

$$(1) \quad Ku = f$$

is the most time consuming computation of the FE simulation. In this equation u represents the change of displacement of the nodes in the FE meshes and f the force unbalance in the system, which is determined by the difference of the internal forces within the system and the external forces exerted on the system. The internal forces are computed by solving non-linear equations for each finite element. The computing time and costs are negligible compared to solving linear system (1). The stiffness matrix K is symmetric positive definite for elastic, constrained systems, hence $\forall u \neq 0 : u^T Ku > 0$ and all eigenvalues of K are positive. Within the context of mechanics, $\frac{1}{2}u^T Ku$ is the strain energy stored within the system for displacement vector u , [1]. Energy is defined as a non-negative entity, hence the strain energy must be non-negative also.

3. ON THEORY OF DPCG

3.1. Motivation of rigid body modes deflation. We have shown in [8] that the number of iterations to convergence for preconditioned CG is highly dependent on the number of aggregates in a mixture as well as the ratio of the E moduli. Increasing the number of aggregates introduces correspondingly more (clustered) small eigenvalues in stiffness matrix K . The jumps in the E moduli

are related to the size of the small eigenvalues. We know from [17] that the smallest eigenvalues correspond to the slowly converging components of the solution.

When a matrix K_{unc} represents a rigid body, i.e., an unconstrained mechanical problem (with no essential boundary conditions) the strain energy equals zero for the rigid body displacements as the system remains undeformed and the matrix is positive semi-definite, $\forall u : u^T K_{unc} u \geq 0$. More specifically, the number of rigid body modes of any unconstrained volume equals the number of zero-valued eigenvalues of its corresponding stiffness matrix. When a matrix has zero-valued eigenvalues the kernel $\mathcal{N}(A)$ is non-trivial. Moreover the basis vectors of the kernel of a stiffness matrix represent the principal directions of the rigid body modes. In general, two types of rigid body modes exist: translations and rotations. In three dimensions this implies six possible rigid body modes and hence six kernel vectors can be associated with the rigid body modes.

For any finite element computation we consider subsets of unconstrained elements as rigid bodies. Their corresponding (sub) stiffness matrices are assemblies of the element stiffness matrices. In the context of asphalt concrete the aggregates are sub-sets of elements, with their E modulus as a shared property, as well as the bitumen and the air voids.

In [8] we conclude that the number of aggregates times the number of rigid body modes per aggregate (6 in three dimensions) is equal to the number of small eigenvalues of stiffness matrix K . By using the deflation technique we augment the Krylov subspace with pre-computed rigid body modes of the aggregates and remove all corresponding small eigenvalues from the system. As a result the number of iterations of the Deflated Preconditioned Conjugated Gradient method is nearly not affected by jumps in material stiffness or by the number of aggregates.

3.2. Recursively Deflated PCG. For the description of deflation we split the solution of (1) into two parts [5]

$$(2) \quad u = (I - P^T)u + P^T u,$$

and let us define the projection P by,

$$(3) \quad P = I - KZ(Z^T KZ)^{-1}Z^T, \quad Z \in \mathbb{R}^{n \times m}$$

where Z is the deflation subspace, i.e., the space to be projected out of the system, and I is the identity matrix of appropriate size. We assume that $m \ll n$ and Z has rank m . Under this assumption $K_c \equiv Z^T KZ$ is symmetric positive definite and may be easily computed and factored. Hence,

$$(4) \quad (I - P^T)u = ZK_c^{-1}Z^T Ku = ZK_c^{-1}Z^T f$$

can be computed immediately. We only need to compute $P^T u$. Because KP^T is symmetric,

$$(5) \quad KP^T = PK,$$

we solve the deflated system,

$$(6) \quad PK\hat{u} = Pf$$

for \hat{u} using the CG method and multiply the result by P^T . We should note that (6) is singular. However, the projected solution $P^T \hat{u}$ is unique, it has no components in the null space, $\mathcal{N}(PK) = \text{span}\{Z\}$. Moreover, from [9], [17] we learn that the null space of PK never enters the iteration process and the corresponding zero-eigenvalues do not influence the solution.

The definition of P given by (3) does not provide insight in the effect of individual deflation vectors on the spectrum of PK . The next theorem defines a recursive deflation operator which

can be used for more extensive eigenvalue analysis of PK . Moreover, it will justify our choice of deflation vectors on which we elaborate later.

Definition 3.1. $P^{(k)} = I - KZ_k(Z_k^T K Z_k)^{-1} Z_k^T$ with $Z_k = [\tilde{Z}_1, \tilde{Z}_2, \dots, \tilde{Z}_k]$, where $\tilde{Z}_j \in \mathbb{R}^{n \times l_j}$ and has rank l_j .

Theorem 3.1. Let $P^{(k)}$ and Z_k as in Definition 3.1, then $P^{(k)}K = P_k P_{k-1} \dots P_1 K$ where $P_{i+1} = I - \tilde{K}_i \tilde{Z}_{i+1} (\tilde{Z}_{i+1}^T \tilde{K}_i \tilde{Z}_{i+1})^{-1} \tilde{Z}_{i+1}^T$, $\tilde{K}_i = P_i \tilde{K}_{i-1}$, $\tilde{K}_1 = P_1 K$, $\tilde{K}_0 = K$, $\tilde{Z}_i^T \tilde{K}_{i-1} \tilde{Z}_i^T$ and $Z_i^T K Z_i$ are non-singular because Z_i are of full rank and K is a symmetric positive definite matrix.

Proof. by induction,

- i. show $P_1 K = P^{(1)} K$ where $Z_1 = \tilde{Z}_1 \in \mathbb{R}^{n \times l_1}$,
- ii. assume $P_{i-1} \tilde{K}_{i-2} = \tilde{K}_{i-1} = P^{(i-1)} K$ where $Z_{i-1} = [\tilde{Z}_{i-1}, \tilde{Z}_{i-2}, \dots, \tilde{Z}_1]$, show that $P_i \tilde{K}_{i-1} = P^{(i)} K$ where $Z_i = [\tilde{Z}_i, Z_{i-1}]$, $Z_{i-1} \in \mathbb{R}^{n \times l(i-1)}$, $\tilde{Z}_i \in \mathbb{R}^{n \times l_i}$ and $l = \sum_{r=i}^1 l_r$.

For the start of the induction we have to prove [i.]. The induction hypothesis is given by [ii.]. We first show that $P_1 K = P^{(1)} K$,

$$\begin{aligned} P_1 K &= K - K \tilde{Z}_1 (\tilde{Z}_1^T K \tilde{Z}_1)^{-1} \tilde{Z}_1^T K \\ &= K - K Z_1 (Z_1^T K Z_1)^{-1} Z_1^T K \\ &= P^{(1)} K. \end{aligned}$$

which implies that (i.) is proved. For (ii.) we assume $P_{i-1} \tilde{K}_{i-2} = P^{(i-1)} K$, and prove that this implies $P_i \tilde{K}_{i-1} = P^{(i)} K$,

$$\begin{aligned} P^{(i)} K &= K - K Z_i (Z_i^T K Z_i)^{-1} Z_i^T K \\ &= K - \begin{bmatrix} K Z_{i-1} & K \tilde{Z}_i \end{bmatrix} \left(\begin{bmatrix} Z_{i-1}^T \\ \tilde{Z}_i^T \end{bmatrix} \begin{bmatrix} K Z_{i-1} & K \tilde{Z}_i \end{bmatrix} \right)^{-1} \begin{bmatrix} Z_{i-1}^T K \\ \tilde{Z}_i^T K \end{bmatrix} \\ (7) \quad &= K - \begin{bmatrix} K Z_{i-1} & K \tilde{Z}_i \end{bmatrix} E^{-1} \begin{bmatrix} Z_{i-1}^T K \\ \tilde{Z}_i^T K \end{bmatrix} \end{aligned}$$

where,

$$E = \begin{bmatrix} Z_{i-1}^T K Z_{i-1} & Z_{i-1}^T K \tilde{Z}_i \\ \tilde{Z}_i^T K Z_{i-1} & \tilde{Z}_i^T K \tilde{Z}_i \end{bmatrix}$$

The matrix $E = \begin{bmatrix} E_{11} & E_{12} \\ E_{21} & E_{22} \end{bmatrix}$ is a symmetric 2x2 block matrix. Its inverse is defined as follows [12],

$$E^{-1} = \begin{bmatrix} E_{11}^{-1} + E_{11}^{-1} E_{12} (E_{22} - E_{21} E_{11}^{-1} E_{21} E_{11}^{-1})^{-1} & -E_{11}^{-1} E_{12} (E_{22} - E_{21} E_{11}^{-1} E_{21} E_{11}^{-1})^{-1} \\ -(E_{22} - E_{21} E_{11}^{-1} E_{21} E_{11}^{-1})^{-1} E_{21} E_{11}^{-1} & (E_{22} - E_{21} E_{11}^{-1} E_{21} E_{11}^{-1})^{-1} \end{bmatrix}$$

with,

$$\Psi = \tilde{Z}_i^T K \tilde{Z}_i - \tilde{Z}_i^T K Z_{i-1} (Z_{i-1}^T K Z_{i-1})^{-1} Z_{i-1}^T K \tilde{Z}_i$$

it follows that

$$\begin{aligned}
(E^{-1})_{11} &= (Z_{i-1}^T K Z_{i-1})^{-1} + (Z_{i-1}^T K Z_{i-1})^{-1} Z_{i-1}^T K \tilde{Z}_i \Psi^{-1} \tilde{Z}_i^T K Z_{i-1} (Z_{i-1}^T K Z_{i-1})^{-1} \\
(E^{-1})_{12} &= - (Z_{i-1}^T K Z_{i-1})^{-1} Z_{i-1}^T K \tilde{Z}_i \Psi^{-1} \\
(E^{-1})_{21} &= -\Psi^{-1} \tilde{Z}_i^T K Z_{i-1} (Z_{i-1}^T K Z_{i-1})^{-1} \\
(E^{-1})_{22} &= \Psi^{-1}
\end{aligned}$$

substitute this into (7) leads to,

$$\begin{aligned}
P^{(i)} K &= K - \begin{bmatrix} K Z_{i-1} & K \tilde{Z}_i \end{bmatrix} \begin{bmatrix} E_{11}^{-1} Z_{i-1}^T K + E_{12}^{-1} \tilde{Z}_i^T K \\ E_{21}^{-1} Z_{i-1}^T K + E_{22}^{-1} \tilde{Z}_i^T K \end{bmatrix} \\
&= K - \begin{bmatrix} K Z_{i-1} E_{11}^{-1} Z_{i-1}^T K + K Z_{i-1} E_{12}^{-1} \tilde{Z}_i^T K + K \tilde{Z}_i E_{21}^{-1} Z_{i-1}^T K + K \tilde{Z}_i E_{22}^{-1} \tilde{Z}_i^T K \end{bmatrix} \\
(8) \quad &= K - K Z_{i-1} (Z_{i-1}^T K Z_{i-1})^{-1} Z_{i-1}^T K \\
&\quad - K Z_{i-1} (Z_{i-1}^T K Z_{i-1})^{-1} Z_{i-1}^T K \tilde{Z}_i \Psi^{-1} \tilde{Z}_i^T K Z_{i-1} (Z_{i-1}^T K Z_{i-1})^{-1} Z_{i-1}^T K \\
&\quad + K Z_{i-1} (Z_{i-1}^T K Z_{i-1})^{-1} Z_{i-1}^T K \tilde{Z}_i \Psi^{-1} \tilde{Z}_i^T K \\
&\quad + K \tilde{Z}_i \Psi^{-1} \tilde{Z}_i^T K Z_{i-1} (Z_{i-1}^T K Z_{i-1})^{-1} Z_{i-1}^T K \\
&\quad - K \tilde{Z}_i \Psi^{-1} \tilde{Z}_i^T K
\end{aligned}$$

In order to show $P_i \tilde{K}_{i-1} = P^{(i)} K$ we now elaborate $P_i \tilde{K}_{i-1}$,

$$\begin{aligned}
P_i \tilde{K}_{i-1} &= \tilde{K}_{i-1} - \tilde{K}_{i-1} \tilde{Z}_i \left(\tilde{Z}_i^T \tilde{K}_{i-1} \tilde{Z}_i \right)^{-1} \tilde{Z}_i^T \tilde{K}_{i-1} \\
&= P^{(i-1)} K - P^{(i-1)} K \tilde{Z}_i \left(\tilde{Z}_i^T P^{(i-1)} K \tilde{Z}_i \right)^{-1} \tilde{Z}_i^T P^{(i-1)} K \\
&= K - K Z_{i-1} (Z_{i-1}^T K Z_{i-1})^{-1} Z_{i-1}^T K \\
&\quad - \left(K - K Z_{i-1} (Z_{i-1}^T K Z_{i-1})^{-1} Z_{i-1}^T K \right) \tilde{Z}_i \cdot \\
&\quad \left(\tilde{Z}_i^T \left(K - K Z_{i-1} (Z_{i-1}^T K Z_{i-1})^{-1} Z_{i-1}^T K \right) \tilde{Z}_i \right)^{-1} \cdot \\
&\quad \tilde{Z}_i^T \left(K - K Z_{i-1} (Z_{i-1}^T K Z_{i-1})^{-1} Z_{i-1}^T K \right) \\
&= K - K Z_{i-1} (Z_{i-1}^T K Z_{i-1})^{-1} Z_{i-1}^T K \\
&\quad - \left(K \tilde{Z}_i - K Z_{i-1} (Z_{i-1}^T K Z_{i-1})^{-1} Z_{i-1}^T K \tilde{Z}_i \right) \cdot \Psi^{-1} \cdot \\
&\quad \left(\tilde{Z}_i^T K - \tilde{Z}_i^T K Z_{i-1} (Z_{i-1}^T K Z_{i-1})^{-1} Z_{i-1}^T K \right) \\
(9) \quad &= K - K Z_{i-1} (Z_{i-1}^T K Z_{i-1})^{-1} Z_{i-1}^T K \\
&\quad - K Z_{i-1} (Z_{i-1}^T K Z_{i-1})^{-1} Z_{i-1}^T K \tilde{Z}_i \Psi^{-1} \tilde{Z}_i^T K Z_{i-1} (Z_{i-1}^T K Z_{i-1})^{-1} Z_{i-1}^T K \\
&\quad + K Z_{i-1} (Z_{i-1}^T K Z_{i-1})^{-1} Z_{i-1}^T K \tilde{Z}_i \Psi^{-1} \tilde{Z}_i^T K \\
&\quad + K \tilde{Z}_i \Psi^{-1} \tilde{Z}_i^T K Z_{i-1} (Z_{i-1}^T K Z_{i-1})^{-1} Z_{i-1}^T K \\
&\quad - K \tilde{Z}_i \Psi^{-1} \tilde{Z}_i^T K
\end{aligned}$$

note that (8) and (9) are identical, so $P_i \tilde{K}_{i-1} = P^{(i)}K$. □

Theorem 3.1 provides us with a theoretical framework in which we construct the deflation vectors. We will see that by subsequently adding rigid body modes of particular sets of elements to the deflation space the number of small eigenvalues of the deflated system is smaller compared to the non-deflated system.

3.3. Condition numbers of Deflated matrices. Let us denote the i th eigenvalue of K in non-decreasing order by $\lambda_i(K)$ or simply by λ_i . Theorem 10.2.6 in [6] provides a bound on the error of CG. After k iterations of the CG method, the error is bounded by,

$$\|u - u_k\|_K \leq 2\|u - u_0\|_K \left(\frac{\sqrt{\kappa} - 1}{\sqrt{\kappa} + 1} \right)^k$$

where $\kappa = \kappa(K) = \frac{\lambda_n}{\lambda_1}$ is the spectral condition number of K , and the K -norm of u is given by $\|u\|_K = \sqrt{u^T K u}$.

To obtain a useful bound for the error of CG for positive semi-definite matrices we define the effective condition number of a semi-definite matrix $D \in \mathbb{R}^{n \times n}$ with corank m to be the ratio of the largest and smallest positive eigenvalue,

$$(10) \quad \kappa_{\text{eff}}(D) = \frac{\lambda_n}{\lambda_{m+1}}.$$

Theorem 2.2 from [5] here repeated as Theorem 3.2 implies that a bound on the condition number of $P^{(k)}K$ can be obtained.

Theorem 3.2. *Let $P^{(k)}$ as defined in Definition 3.1 and suppose there exists a splitting $K = C + R$ such that C and R are symmetric positive semi-definite with $\mathcal{N}(C) = \text{span}\{Z_k\}$ the null space of C . Then for ordered eigenvalues λ_i ,*

$$(11) \quad \lambda_i(C) \leq \lambda_i(P^{(k)}K) \leq \lambda_i(C) + \lambda_{\max}(P^{(k)}R).$$

Moreover, the effective condition number of $P^{(k)}K$ is bounded by,

$$(12) \quad \kappa_{\text{eff}}(P^{(k)}K) \leq \frac{\lambda_n(K)}{\lambda_{m+1}(C)}.$$

Proof. See [5] (p445). □

The large discontinuities in matrix entries due to strongly varying material properties in the FE discretization induce unfavorable eigenvalues (either large or small) in the spectrum of stiffness matrix K . The effective condition number of $P^{(k)}K$ is bounded by the smallest eigenvalue of C and the largest eigenvalue of K . To remove the discontinuities and thus eliminating those unfavorable eigenvalues we decouple the sub-matrices of stiffness matrix K that correspond to different materials by finding the correct splitting. The eigenvalues of the decoupled sub-matrices determine the spectrum of $P^{(k)}K$. However, due to the large differences in stiffness the value of the eigenvalues for different sub-matrices can vary over several order of magnitudes. We use a preconditioner to map the spectra of the sub-matrices onto the same region, around 1. The deflation technique can be used in conjunction with ordinary preconditioning techniques such as diagonal scaling or Incomplete Cholesky factorization. This is a two-level approach, treating the smallest

eigenvalues and largest eigenvalues by deflation and preconditioning respectively. By choosing a smart combination of deflation and preconditioning a more favorable spectrum is obtained, yielding a smaller condition number and less iterations. For a symmetric preconditioner $M = LL^T$, e.g. diagonal scaling, we extend the result of Theorem 3.2 to

$$(13) \quad \kappa_{\text{eff}}(L^{-1}P^{(k)}KL^{-T}) \leq \frac{\lambda_n(L^{-1}KL^{-T})}{\lambda_{m+1}(L^{-1}CL^{-T})}.$$

4. RECURSIVE DEFLATION FOR FE PROBLEMS

4.1. Recursive Deflation strategy. In this section we introduce a strategy to construct the deflation space Z_j for $P^{(j)}K$ of Definition 3.1 to obtain decoupled problems using Theorems 3.2 and 3.1. Our starting point is by observing that null spaces of sets of elements are represented by the rigid body modes of those sets of elements. By choosing sets of elements we define C and the nullspace of C is our deflation space, which is by definition spanned by the rigid body modes. In Appendix A an algorithm is given for computing rigid body modes of sets of elements.

We have an arbitrary FE mesh Ω consisting of elements e_i , $i = 1, \dots, n$ and m materials, sorted by decreasing stiffness. We will elaborate on the importance of the ordering by material stiffness in Section 4.2. Material j of the FE mesh can have multiple bodies j_k which is the collection of connected elements that share the same material property. We note that each body of material induces a jump in the entries of the stiffness matrix of which the size depends on the differences in stiffness of the corresponding materials. Hence it is important to distinguish all bodies of all materials as we want to decouple those regions in the stiffness matrix. The set of elements that makes up a body l of the material j is defined as Ω_j^l , where $\Omega = \bigcup_{j=1}^m \{\bigcup_{l=1}^{j_k} \Omega_j^l\}$. Let $\mathcal{I} = \{i : e_i \subset \Omega\}$ be defined as the index set of Ω . The index set of Ω_j^l is $\mathcal{I}_j^l = \{i : e_i \subset \Omega_j^l\}$. We also define index set $\mathcal{I}_j^{l,\Gamma} = \{i : (e_i \subset \Omega \setminus \Omega_j^l) \wedge (e_i \cap e_k \neq \emptyset, \forall e_k \subset \Omega_j^l)\}$, which contains all indices of the elements of $\Omega \setminus \Omega_j^l$ that are connected to (the boundary elements of) Ω_j^l .

Start with material $j = 1$ and body $l = 1$, which corresponds to sub-mesh Ω_1^1 . This yields the first splitting:

$$\begin{aligned} \tilde{K}_0 &= A = C_0 + R_0 \\ C_0 &= \sum_{i \in \mathcal{I}_1^1} N_{e_i}^T K_{e_i} N_{e_i} + \sum_{i \in \mathcal{I} \setminus \{\mathcal{I}_1^{1,\Gamma} \cup \mathcal{I}_1^1\}} N_{e_i}^T K_{e_i} N_{e_i} \\ R_0 &= \sum_{i \in \mathcal{I}_1^{1,\Gamma}} N_{e_i}^T K_{e_i} N_{e_i} \end{aligned}$$

The matrix C_0 consists of the assembly of all finite elements that belong to body $l = 1$ of material $j = 1$. Matrix K_{e_i} is the element stiffness matrix of element e_i with corresponding connectivity matrix N_{e_i} . The matrix R_0 consists of the assembly of all finite elements that share nodes with the elements on the boundary of body $l = 1$ of material $j = 1$ but that are not contained within sub-mesh Ω_1^1 . The first splitting yields, $\mathcal{N}(C_0) = \tilde{Z}_1$ and $P_1 = I - \tilde{A}_0 \tilde{Z}_1 (\tilde{Z}_1^T \tilde{A}_0 \tilde{Z}_1)^{-1} \tilde{Z}_1^T$. By this splitting we have decoupled the first body of material 1 from all other materials. The rigid body modes of all elements corresponding to the first body of material 1 are contained in $\mathcal{N}(C_0)$. We construct $\tilde{A}_1 = P_1 A = P_1 (C_0 + R_0) = P_1 C_0 + P_1 R_0 = C_0 + \tilde{R}_0$, where $P_1 C_0 = C_0$ follows by definition of P_1 . Continuing with the second body of material 1 and repeating the previous

decoupling step gives

$$\begin{aligned}\tilde{K}_1 &= P_1 A = C_0 + \tilde{R}_0 = C_1 + R_1 + \tilde{R}_0 \\ C_1 &= \sum_{i \in \mathcal{I}_1^1} N_{e_i}^T K_{e_i} N_{e_i} + \sum_{i \in \mathcal{I}_1^2 \setminus \mathcal{I}_1^{1,\Gamma}} N_{e_i}^T K_{e_i} N_{e_i} + \sum_{i \in \mathcal{I} \setminus \bigcup_{i=1}^2 \{\mathcal{I}_1^{l,\Gamma} \cup \mathcal{I}_1^i\}} N_{e_i}^T K_{e_i} N_{e_i} \\ R_1 &= \sum_{i \in \mathcal{I}_1^2 \setminus \mathcal{I}_1^{1,\Gamma}} N_{e_i}^T K_{e_i} N_{e_i}\end{aligned}$$

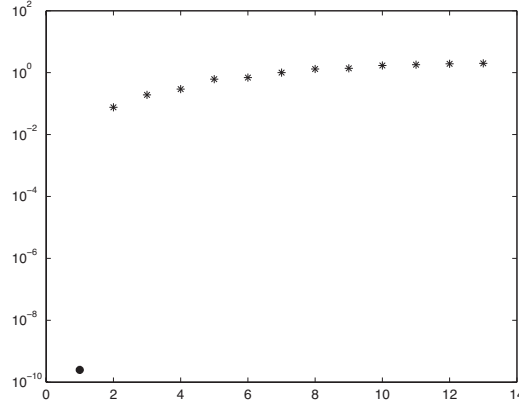
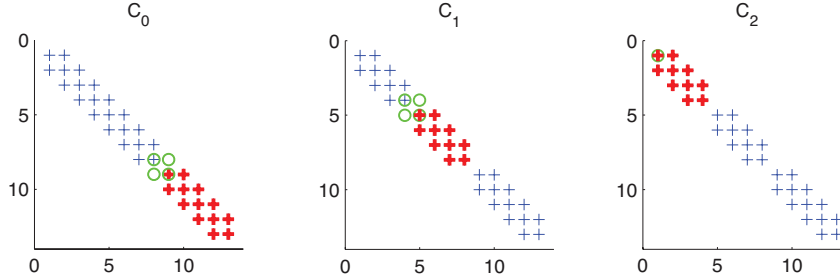
Hence, $\mathcal{N}(C_1) = \tilde{Z}_2$ and $P_2 = I - \tilde{A}_1 \tilde{Z}_2 (\tilde{Z}_2^T \tilde{A}_1 \tilde{Z}_2)^{-1} \tilde{Z}_2^T$. Continue for all bodies and materials. At splitting $m = \sum_{j=1}^{n-1} j_k + l$ for material n and body l ,

$$\begin{aligned}\tilde{K}_{m-1} &= C_{m-2} + \tilde{R}_{m-2} = C_{m-1} + R_{m-1} + \tilde{R}_{m-2} \\ C_{m-1} &= \sum_{q=1}^{n-1} \left[\sum_{r=1}^{q_k} \left[\sum_{i \in \mathcal{P}} N_{e_i}^T K_{e_i} N_{e_i} \right] \right] \\ &\quad + \sum_{r=1}^l \left[\sum_{i \in \mathcal{C}} N_{e_i}^T K_{e_i} N_{e_i} \right] \\ &\quad + \sum_{i \in \mathcal{U}} N_{e_i}^T K_{e_i} N_{e_i} \\ R_{m-1} &= \sum_{i \in \mathcal{B}} N_{e_i}^T K_{e_i} N_{e_i}\end{aligned}$$

where,

$$\begin{aligned}\mathcal{P} &= \mathcal{I}_q^r \setminus \left\{ \bigcup_{j=1}^{q-1} \bigcup_{s=1}^{j_k} \mathcal{I}_j^{s,\Gamma} \right\} \\ \mathcal{C} &= \mathcal{I}_n^r \setminus \left\{ \bigcup_{j=1}^{n-1} \bigcup_{s=1}^{j_k} \mathcal{I}_j^{s,\Gamma} \right\} \cup \left\{ \bigcup_{s=1}^{l-1} \mathcal{I}_n^{s,\Gamma} \right\} \\ \mathcal{U} &= \mathcal{I} \setminus \left\{ \bigcup_{q=1}^{n-1} \left\{ \bigcup_{r=1}^{q_k} \mathcal{I}_q^{r,\Gamma} \cup \mathcal{I}_q^r \right\} \right\} \cup \left\{ \bigcup_{r=1}^l \mathcal{I}_n^{r,\Gamma} \cup \mathcal{I}_n^r \right\} \\ \mathcal{B} &= \mathcal{I}_n^{l,\Gamma} \setminus \left\{ \bigcup_{j=1}^{n-1} \bigcup_{s=1}^{j_k} \mathcal{I}_j^{s,\Gamma} \right\} \cup \left\{ \bigcup_{s=1}^{l-1} \mathcal{I}_n^{s,\Gamma} \right\}\end{aligned}$$

Hence, $\mathcal{N}(C_{m-1}) = \tilde{Z}_m$ and $P_{m-1} = I - \tilde{K}_{m-1} \tilde{Z}_m (\tilde{Z}_m^T \tilde{K}_{m-1} \tilde{Z}_m)^{-1} \tilde{Z}_m^T = P$ with $P = I - AZ(Z^T AZ)^{-1} Z^T$ and $\text{span}\{Z\} = \bigcup_{j=1}^m \text{span}\{\tilde{Z}_j\}$. The above expression for \tilde{K}_{m-1} is rather complex. We have divided the index sets needed for assembly of C_{m-1} and R_{m-1} into 4 sub-sets, \mathcal{P} , \mathcal{C} , \mathcal{U} and \mathcal{B} . The set \mathcal{P} contains all element indices that belong to body r of material q except for all elements that are included in boundary element sets of previously assembled materials and bodies. The set \mathcal{C} contains all the element indices that belong to body r of current material n except for all elements that are included in boundary element sets of previously assembled materials and bodies, and the $l-1$ assembled bodies of the current material. The set \mathcal{U} contains all the element indices that belong to materials and bodies that have not been assembled yet. The set \mathcal{B} contains all

FIGURE 1. spectrum of $M^{-1}K$ where $[c_1, c_2, c_3] = [1, 10^4, 10^8]$.FIGURE 2. sparsity pattern C_0 , C_1 and C_2 . Nonzero elements represented by symbols; corresponding to deflated material, interface elements and remaining elements pictured by bold crosses, circles and non bold crosses respectively.

The spectrum of $M^{-1}K$ is given by Figure 1. Clearly the smallest eigenvalue, which is of $\mathcal{O}(10^{-10})$ and induced by the (only real) rigid body contained in the mesh, is much smaller compared to the other eigenvalues. Moreover, it affects the condition number of $M^{-1}K$. Now we apply the deflation strategy by finding a correct splitting of K . We sort the materials in decreasing order of diffusion. Figure 2 shows the sparsity pattern of the three splitting matrices C_0 , C_1 and C_2 . In matrix C_0 the assembly of the elements belonging to stiffest material 3, is represented by the bold crosses. The interface between weaker material 2 and 3, which goes to R_0 , is represented by the circles and all other elements are represented by the non bold crosses. The second splitting is the decoupling of material 2 from the system, again those elements are represented by the bold crosses. The interface between material 2 and 3 has been removed already, the interface between material 2 and 1 goes to R_1 . The remaining splitting is the decoupling of material 1 from the boundary conditions which go to R_2 .

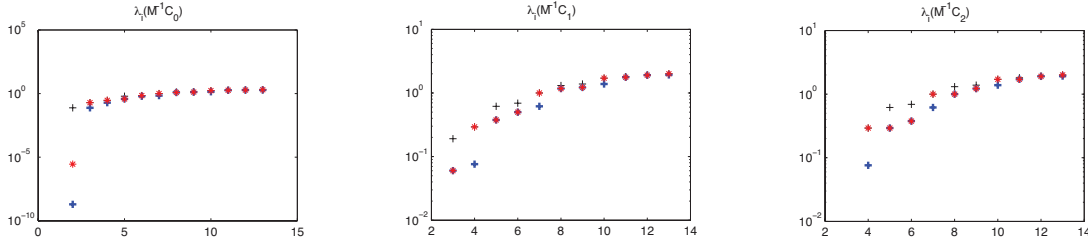


FIGURE 3. spectrum of $M^{-1}C_i$ (\star correct, $\boldsymbol{+}$ wrong choice deflation vectors) compared to spectrum of $M^{-1}K$ ($+$)

4.2. Deflation vectors in the neighborhood of a jump. If some elements of a less stiff material are assigned to the element set of a stiffer material, the material stiffness matrices are not decoupled. We illustrate this with a simple example. When a node belongs to two elements and two different materials and is assigned to the wrong (least stiff) element with respect to the splitting of K , then by applying the preconditioner the coupling between the stiffness matrices remains. For instance, the 1D Poisson problem and preconditioning based on diagonal scaling, the entry on the main diagonal is $c_1 + c_2$, with $c_1 \ll c_2$. Clearly, when decoupled correctly, we have in splitting of K only c_2 on the main diagonal of C , hence $M^{-1}C$ gives $\frac{c_2}{c_1+c_2} \approx 1$. With a wrong choice of deflation vectors, we have c_1 on the main diagonal of C , hence $M^{-1}C$ gives $\frac{c_1}{c_1+c_2} \approx \frac{1}{c_2} \ll 1$. However all other terms on the diagonal of $M^{-1}C$ will be approximately 1, introducing small eigenvalues for this material and unfavorable local spectrum of eigenvalues of $M^{-1}C$.

4.2.1. Illustrative example: 1D Poisson equation (continued). We illustrate the effect of incorrect decoupling by analyzing the spectrum of the splitting matrices for the 1D Poisson equation. Figure 3 shows the spectrum of $M^{-1}C_i$ for the correct (star) and wrong (bold cross) choice of deflation vectors compared to the spectrum of $M^{-1}K$. After applying three deflation operations, we observe from the spectrum of $M^{-1}C_2$ that the smallest eigenvalue of the wrong choice of deflation vectors is much smaller than the smallest eigenvalue for the correct choice of deflation vectors, which coincides with the smallest eigenvalue value in the spectrum of $M^{-1}K$. Moreover, we can see from the spectrum of C_0 and C_1 that the wrong choice is clearly been made with respect to coupling of material 3 and material 2. The effective condition number of the wrong choice of deflation vectors will affect the performance of DPCG. Figure 4 shows the convergence of the error of DPCG and PCG for correct(+) and wrong(-) choice of deflation vectors. The performance of DPCG(-) is worse than DPCG(+), as predicted by values of the eigenvalues in Figure 3.

4.3. DPCG algorithm. The deflation method was proposed by [13]. A practical variant of the Deflated Preconditioned Gradient Method from [16] is given by Algorithm 1.

4.3.1. Additional work DPCG. The projector P is never computed explicitly. We compute the sparse matrix $K_Z = KZ$ as well as the inverse of the small dense matrix $E = Z^T K_Z$ beforehand. Assume the (full rank) deflation space has dimension $d \ll n$ where $K \in \mathcal{R}^{n \times n}$ implying $Z \in \mathcal{R}^{n \times d}$, $E \in \mathcal{R}^{d \times d}$ and $K_Z \in \mathcal{R}^{n \times d}$. Evaluation of $w = Pv$ is equal to $w = v - K_Z E^{-1} Z^T v$. Stiffness matrix K , deflation vectors Z and matrix K_Z are sparse. We compare the cost of one matrix

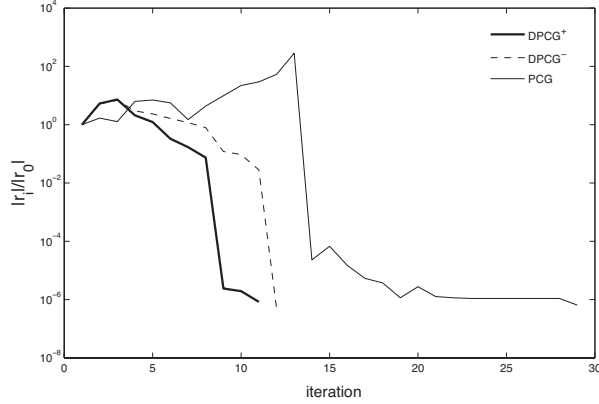


FIGURE 4. Convergence of DPCG and PCG where $[c_1, c_2, c_3] = [1, 10^4, 10^8]$ and DPCG⁺, DPCG⁻ represent correct and wrong choice of deflation vectors respectively.

Algorithm 1 Deflated preconditioned CG solving $K\mathbf{u} = \mathbf{f}$

```

Select  $\mathbf{u}_0$ . Compute  $\mathbf{r}_0 = (\mathbf{f} - K\mathbf{u}_0)$ , set  $\hat{\mathbf{r}}_0 = P\mathbf{r}_0$  and  $\mathbf{p}_0 = \hat{\mathbf{r}}_0$ 
Solve  $M\mathbf{y}_0 = \hat{\mathbf{r}}_0$  and set  $\mathbf{p}_0 = \mathbf{y}_0$ 
for  $j = 0, 1, \dots$  until convergence do
   $\hat{\mathbf{w}}_j = PK\mathbf{p}_j$ 
   $\alpha_j = \frac{(\hat{\mathbf{r}}_j, \mathbf{y}_j)}{(\hat{\mathbf{w}}_j, \mathbf{p}_j)}$ 
   $\hat{\mathbf{u}}_{j+1} = \hat{\mathbf{u}}_j + \alpha_j \mathbf{p}_j$ 
   $\hat{\mathbf{r}}_{j+1} = \hat{\mathbf{r}}_j - \alpha_j \hat{\mathbf{w}}_j$ 
  Solve  $M\mathbf{y}_{j+1} = \hat{\mathbf{r}}_{j+1}$ 
   $\beta_j = \frac{(\hat{\mathbf{r}}_{j+1}, \mathbf{y}_{j+1})}{(\hat{\mathbf{r}}_j, \mathbf{y}_j)}$ 
   $\mathbf{p}_{j+1} = \mathbf{y}_{j+1} + \beta_j \mathbf{p}_j$ 
end for
 $\mathbf{u} = ZK_c^{-1}Z^T\mathbf{f} + P^T\hat{\mathbf{u}}_{j+1}$ 

```

vector product of the stiffness matrix K and the deflation matrix P by comparing the number of flops. Assume that the average number of nonzeros for each row of K , Z^T and K_Z is α , β and γ respectively. The total number of flops of one matrix vector multiplication with stiffness matrix K is $2\alpha n$. The (cumulative) number of flops of P is $(2\beta d) + (2d^2) + (2\gamma n) + n$, clearly $2\gamma n$ is the dominating term but is difficult to estimate as γ depends on the number of deflation vectors. However, if the number of deflation vectors is small and Z very sparse, the number of nonzeros in K_Z will be comparable to the number of nonzeros of K and the number of flops of both operators will be of the same order of magnitude. Choosing dense deflation vectors with much overlap may cause operator P to be more expensive than K in terms of flops.

5. NUMERICAL EXPERIMENTS

Both experiments in this section concern the analysis of asphaltic materials subjected to an external force. These materials give rise to coupled partial differential equations [4]. The experiments make use of the same set of material parameters. We distinguish between three materials: aggregates, bitumen, and air voids. The corresponding stiffness coefficients (E modulus) are given

in Table 1 and are the dominating contributions to the entries of the stiffness matrix. In order to illustrate the effect of the discontinuities on the convergence of PCG, we show results for 4 sets of parameters. The first set (i.) from Table 1 contains realistic material parameters. The other sets do not have a direct physical meaning to asphaltic materials, but are used for illustration of the performance of deflation. We have conducted the experiments with two different preconditioners, diagonal scaling and Incomplete Cholesky with a drop tolerance of 10^{-2} . This drop tolerance was determined after performing several tests with ILUPACK [2] and represents the optimal value in terms of memory usage (lower drop tolerance demands more memory) and the speed of the back solve (lower tolerance yields a slower back solve) against the performance of the preconditioner in terms of reduction in number of iterations of DPCG. We have implemented PCG and DPCG into the existing parallel FE software package CAPA-3D [3]. All experiments were done on a cluster of Dell workstations containing 8 CPUs Intel Xeon E5450, running at 3.00GHz and connected by Infiniband.

TABLE 1. E modulus for different materials

	aggregate	bitumen	air voids
i.	69000	5000	100
ii.	690000	5000	100
iii.	69000	500	100
iv.	69000	5000	10^{-2}

5.1. Experiment 1: cylinder containing aggregates and bitumen. The case given in Figure 5 is a cylinder of soft material (air voids) containing three aggregates embedded in a layer of bitumen. We compare DPCG and PCG in combination with diagonal scaling. The case involves a mixture of materials that is subjected to an external force applied to the upper boundary of the volume. Zero displacement boundary conditions are imposed on the base of the volume, this is homogenous Dirichlet boundary conditions to all degrees of freedom in the x, z -plane for $y = 0$. We note that the case resembles the uniaxial compression test, which is a standard laboratory test. We observe the convergence behavior of DPCG and PCG for variations in the E modulus of the bitumen and aggregates as given in Table 1. We compare a standard choice for the values of parameter E [4] with increased stiffness of the aggregates, and decreasing stiffness for the bitumen and air voids.

TABLE 2. example 1: CPU wall time(s) PCG and DPCG

	PCG		DPCG	
	iter	cpu (s)	iter	cpu(s)
i.	648	0.288	143	0.204
ii.	1089	0.477	154	0.175
iii.	746	0.328	149	0.172
iv.	1581	0.677	242	0.276

Figure 6 shows the convergence of PCG and DPCG for parameter sets (i.) to (iv.). Clearly the convergence of the solution with PCG is slow and highly oscillating. PCG compared to DPCG is also slower in terms of CPU time. But due to the small problem size, this is more a qualitative example rather than quantitative. We observe in the plots of sets (i.) to (iii.) that the value of

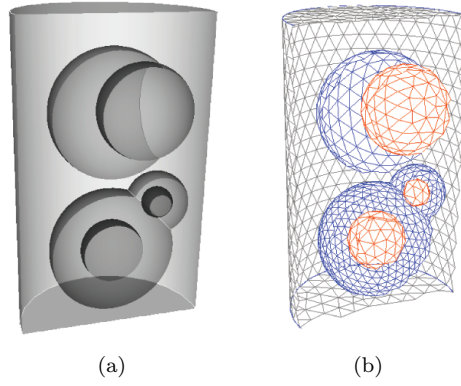


FIGURE 5. FE mesh and schematic representation of cylinder containing three aggregates represented by sphericals

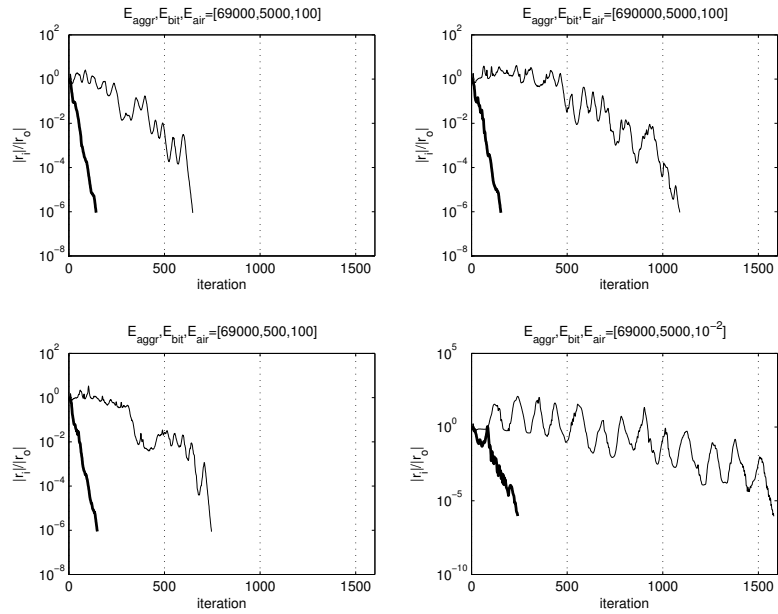


FIGURE 6. Convergence of PCG and DPCG (bold line) for cylinder containing three aggregates

the material stiffness for the aggregates and bitumen does not influence the number of iterations of DPCG. This is what we expected. The stiffness matrices corresponding to the aggregates and bitumen have been decoupled. The effective condition number is bounded by the smallest eigenvalue of the least stiff material, the air voids. This can also be observed in the plot of set (iv). The

number of iterations of DPCG increases from 150 towards 242 for air. As the value of the material stiffness of the air voids changes from 100 to 10^{-2} , the effective condition number increases as well as the number of iterations of both DPCG and PCG. However, this is not surprising as the smallest (non-zero) eigenvalue is determined by the least stiff material, due to the decoupling of the stiffness matrices corresponding to the different materials. When the stiffness decreases, the smallest eigenvalue will become smaller and subsequently the condition number increases. We do not consider this as a shortcoming of the deflation method as it can and must be solved by applying the right preconditioner.

5.2. Experiment 2: FE mesh from CT scan. The case given in Figure 7 is a FE mesh of a real life sample of asphaltic material obtained from CT scan. We compare DPCG and PCG in combination with incomplete Cholesky with drop tolerance 10^{-2} . The case involves a mixture of materials that is subjected to an external force applied to the upper boundary of the volume. Zero displacement boundary conditions are imposed on three sides of the volume, this is homogenous Dirichlet boundary conditions to all degrees of freedom in the x, z -, x, y - and y, z - planes for $y = 0$, $z = 0$ and $x = 0$ respectively. We observe the convergence behavior of DPCG and PCG for variations in the E modulus of the bitumen and aggregates as given in Table 1. We compare a standard choice of parameters [4] with increased stiffness of the aggregates, and decreasing stiffness for the bitumen.

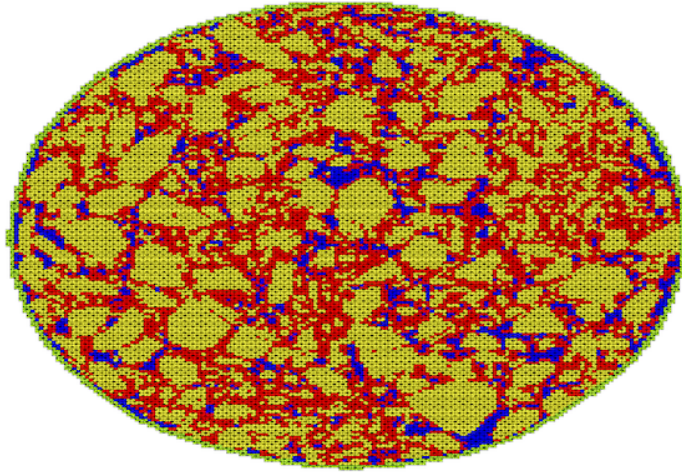


FIGURE 7. FE mesh from CT scan of real slice of asphaltic material

There is a difference between the artificial cylinder and the sample of real asphaltic material. Where it was possible to decouple all materials in case of the cylinder, for a FE mesh obtained from a CT scan this is much more involved. We can see from Figure 8 (b) and (c) that there exist many small bodies of material. Each body is represented in the deflation space by six rigid body modes. However, due to overlap, many of these sparse vectors will become zero, implying a singular deflation matrix. Moreover, because of the large number of small bodies and thus deflation vectors,

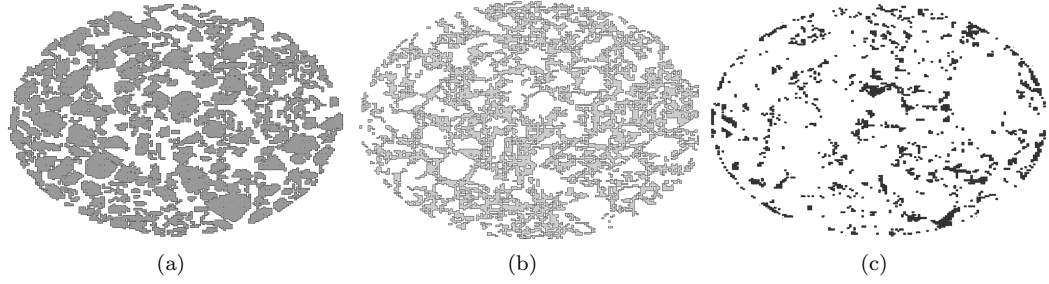


FIGURE 8. deflation strategy, identify sets of elements corresponding to material: (a) aggregates, (b) bitumen and (c) air voids.

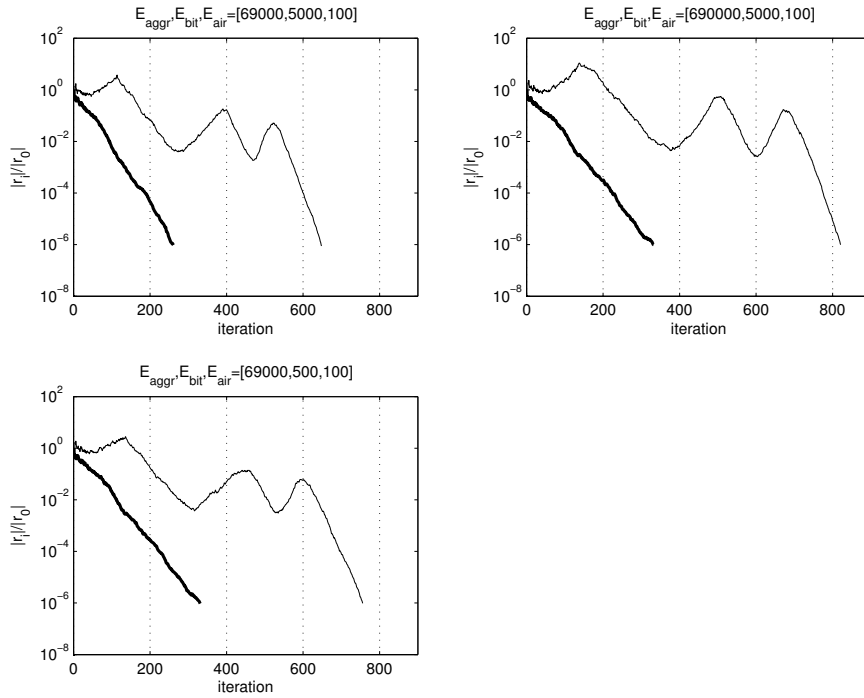


FIGURE 9. Convergence of PCG and DPCG for a real slice of asphaltic material

it would be more favorable in terms of overhead to collapse these bodies into one entity. Therefore we have used an adapted version of the deflation strategy of Section 4.1.1. By combining sets of elements of different materials, we still have a decoupling when we keep in mind the decreasing order of stiffness for the construction of the splitting of Theorem 3.2. We note that we lose some rigid body modes, and hence a worse bound of the condition number for PK but we gain performance because of a large reduction in deflation vectors and avoid singularity of the deflation matrix. Also

TABLE 3. example 2: CPU wall time(s) PCG and DPCG

	PCG		DPCG	
	iter	cpu (s)	iter	cpu(s)
i.	648	13.18	261	7.26
ii.	821	17.48	332	9.31
iii.	756	15.21	331	8.89

we have omitted set (iv.) from this test because the FE software would not run this value of air voids due to collapsing elements (negative Jacobian).

We observe in Figure 8 that PCG has a strongly oscillating path of convergence and DPCG has nearly a straight line. Clearly the unfavorable eigenvalues have been removed by deflation. However, the system is not decoupled completely because the number of iterations is not invariant for different sets of material parameters. But the number of iterations of DPCG is much smaller compared to PCG. The performance of DPCG in terms of CPU walltime is also better compared to PCG.

6. CONCLUSION

We considered the application of the Deflated Preconditioned Conjugate Gradient method to mechanical problems with strongly varying stiffness of materials. We described a simple general applicable way on how to choose deflation vectors by using the rigid body modes of subsets of elements. By combining the deflation technique and the computation of the exact rigid body modes of the components the robust deflated preconditioned gradient method (DPCG) is obtained. The DPCG method is insensitive to large jumps in the E modulus of materials. The amount of work per iteration for the deflation operator of DPCG is comparable to one matrix vector product. However, this does not imply that DPCG becomes twice as expensive as PCG because the preconditioning step consumes most resources in both time and memory. For most applications, using sparse deflation vectors, DPCG is roughly 30% more expensive in time per iteration compared to PCG.

ACKNOWLEDGEMENTS

We would like to thank both referees for their thorough review of our paper which contributed to some important improvements of the original manuscript.

APPENDIX A. COMPUTING RIGID BODY MODES OF A FINITE ELEMENT

We know from [1] that the rigid body modes of a finite element are spanned by the kernel base vectors of the corresponding element stiffness matrix. We will show a fast and cheap solution for the computation of the rigid body modes. The same principle can be easily extended to sets of finite elements of arbitrary shape and order. We note that the rigid body modes are only defined by the geometric properties of the element.

In three dimensions a finite element has 6 rigid body motions; three translations and three rotations. For simplicity we consider a 4 noded tetrahedral element, however all derivations can be extended to N noded elements without loss of generality. The coordinate vector of the element is given by,

$$\{ x_1 \quad y_1 \quad z_1 \quad x_2 \quad y_2 \quad z_2 \quad x_3 \quad y_3 \quad z_3 \quad x_4 \quad y_4 \quad z_4 \}^T$$

A translation can be considered as a uniform displacement of every node in a given direction. To obtain three orthogonal translations we choose the x, y and z direction respectively. The three translation vectors are given by,

$$\begin{aligned} & \{ 1 \ 0 \ 0 \ 1 \ 0 \ 0 \ 1 \ 0 \ 0 \ 1 \ 0 \ 0 \}^T \\ & \{ 0 \ 1 \ 0 \ 0 \ 1 \ 0 \ 0 \ 1 \ 0 \ 0 \ 1 \ 0 \}^T \\ & \{ 0 \ 0 \ 1 \ 0 \ 0 \ 1 \ 0 \ 0 \ 1 \ 0 \ 0 \ 1 \}^T \end{aligned}$$

The rotations can be easily described using the spherical coordinate system,

$$x = r \cos(\theta) \sin(\phi), \quad y = r \sin(\theta) \sin(\phi), \quad z = r \cos(\phi)$$

where

$$r = \sqrt{x^2 + y^2 + z^2}, \quad \theta = \tan^{-1} \left(\frac{y}{x} \right), \quad \phi = \cos^{-1} \left(\frac{z}{r} \right)$$

and θ and ϕ as in Figure 10(a).

We derive a rotation $d\theta$ in the x, y -plane, hence $d\phi = 0$ and $dr = 0$. The x - y , x - z and y - z planes contain unique rotations. The corresponding vectors can be found by swapping axis. For an arbitrary point in space which has spherical coordinates (r, θ, ϕ) a change $d\theta$ in the x, y -plane yields a displacement in cartesian coordinates of,

$$dx = -r \sin(\theta) \sin(\phi) d\theta, \quad dy = r \cos(\theta) \sin(\phi) d\theta, \quad dz = 0.$$

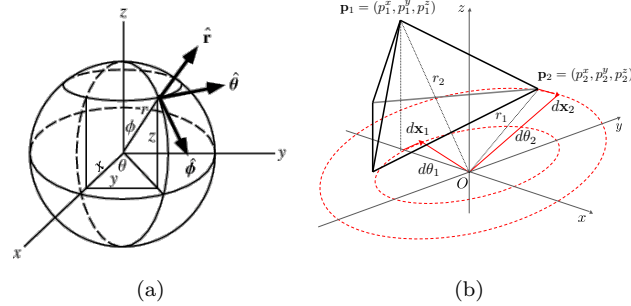


FIGURE 10. (a) spherical coordinates, (b) rotation around origin of tetrahedral element in x, y -plane

Figure 10(b) shows the rotation for one element with respect to the origin over angle $d\theta$. By using above expressions we obtain all three rotation vectors,

rotation x-y plane,

$$\theta_j = \tan^{-1} \left(\frac{y_j}{x_j} \right), \quad \phi_j = \cos^{-1} \left(\frac{z_j}{r_j} \right), \quad \left. \begin{array}{l} -r_1 \sin(\theta_1) \sin(\phi_1) \\ r_1 \cos(\theta_1) \sin(\phi_1) \\ 0 \\ -r_2 \sin(\theta_2) \sin(\phi_2) \\ r_2 \cos(\theta_2) \sin(\phi_2) \\ 0 \\ -r_3 \sin(\theta_3) \sin(\phi_3) \\ r_3 \cos(\theta_3) \sin(\phi_3) \\ 0 \\ -r_4 \sin(\theta_4) \sin(\phi_4) \\ r_4 \cos(\theta_4) \sin(\phi_4) \\ 0 \end{array} \right\}$$

rotation y-z plane,

$$\theta_j = \tan^{-1} \left(\frac{z_j}{x_j} \right), \quad \phi_j = \cos^{-1} \left(\frac{y_j}{r_j} \right), \quad \left\{ \begin{array}{c} -r_1 \sin(\theta_1) \sin(\phi_1) \\ 0 \\ r_1 \cos(\theta_1) \sin(\phi_1) \\ -r_2 \sin(\theta_2) \sin(\phi_2) \\ 0 \\ r_2 \cos(\theta_2) \sin(\phi_2) \\ -r_3 \sin(\theta_3) \sin(\phi_3) \\ 0 \\ r_3 \cos(\theta_3) \sin(\phi_3) \\ -r_4 \sin(\theta_4) \sin(\phi_4) \\ 0 \\ r_4 \cos(\theta_4) \sin(\phi_4) \end{array} \right\}$$

rotation x-z plane,

$$\theta_j = \tan^{-1} \left(\frac{z_j}{y_j} \right), \quad \phi_j = \cos^{-1} \left(\frac{x_j}{r_j} \right), \quad \left\{ \begin{array}{c} 0 \\ r_1 \cos(\theta_1) \sin(\phi_1) \\ -r_1 \sin(\theta_1) \sin(\phi_1) \\ 0 \\ r_2 \cos(\theta_2) \sin(\phi_2) \\ -r_2 \sin(\theta_2) \sin(\phi_2) \\ 0 \\ r_3 \cos(\theta_3) \sin(\phi_3) \\ -r_3 \sin(\theta_3) \sin(\phi_3) \\ 0 \\ r_4 \cos(\theta_4) \sin(\phi_4) \\ -r_4 \sin(\theta_4) \sin(\phi_4) \end{array} \right\}$$

We compute the null space of each element matrix. Sets of elements make up the bodies of materials, as a collection of elements share a certain property and are neighbors. The rigid body modes of a collection of elements is equal to the assembly of the rigid body modes of the individual elements taking into account the multiplicity of those degrees of freedom that lie in multiple neighboring elements. In the case of asphaltic materials we choose the element stiffness as the property for discrimination between elements. We can think of stones, bitumen and air voids. We should note that we compute the rigid body modes of each independent body of material. Hence, two bodies of the same material imply 12 deflation vectors. This has a physical meaning also, two bodies will not rotate and translate at the same time and at the same rate. Therefore these movements need to be taken care of independently.

REFERENCES

- [1] K. J. Bathe. *Finite Element Procedures*. Prentice Hall, 2 revised ed edition, June 1995.
- [2] M. Bollhöfer and Y. Saad. Multilevel preconditioners constructed from Inverse-Based ILUs. *SIAM J. Sci. Comput.*, 27(5):1627–1650, 2006.
- [3] CAPA3D. Capa-3d computer aided pavement analysis. <http://www.capa-3d.org>, 2009.
- [4] A. Drescher, N. Kringos, and A. Scarpas. On the behavior of a parallel elasto-visco-plastic model for asphaltic materials. *Mechanics of Materials*, pages 109–117, 2009.
- [5] J. Frank and C. Vuik. On the construction of deflation-based preconditioners. *SIAM J. Sci. Comput.*, 23(2):442–462, 2001.
- [6] G. H. Golub and C. F. Van Loan. *Matrix Computations (Johns Hopkins Studies in Mathematical Sciences)*. The Johns Hopkins University Press, Baltimore, 1996.
- [7] M. Griebel, D. Oeltz, M. Schweitzer, and A. Schweitzer. An algebraic multigrid method for linear elasticity. *SIAM J. Sci. Comp*, page 407, 2003.
- [8] T.B. Jönsthövel, M.B. van Gijzen, C.Vuik, C. Kasbergen, and A. Scarpas. Preconditioned conjugate gradient method enhanced by deflation of rigid body modes applied to composite materials. *Computer Modeling in Engineering and Sciences*, 47:97–118, 2009.
- [9] E. F. Kaasschieter. Preconditioned conjugate gradients for solving singular systems. *J. Comput. Appl. Math.*, 24(1-2):265–275, 1988.
- [10] A. Klawonn and O.B. Widlund. A domain decomposition method with lagrange multipliers and inexact solvers for linear elasticity. *SIAM J. Sci. Comput.*, 22:1199–1219, 2000.

- [11] A. Klawonn, O.B. Widlund, and D. Maksymilian. Dual-primal feti methods for three-dimensional elliptic problems with heterogeneous coefficients. *SIAM J. Numer. Anal.*, 40:159–179, 2002.
- [12] T. Lu and S. Shiou. Inverses of 2 x 2 block matrices,. *Computers and Mathematics with Applications*, 43(1-2):119 – 129, 2002.
- [13] R. A. Nicolaides. Deflation of conjugate gradients with applications to boundary value problems. *SIAM J. Numer. Anal.*, 24(2):355–365, 1987.
- [14] Simpleware. <http://www.simpleware.com>, 2009.
- [15] J.M. Tang, S.P. MacLachlan, R. Nabben, and C. Vuik. A comparison of two-level preconditioners based on multigrid and deflation. *SIAM. J. Matrix Anal. and Appl.*, 31:1715–1739, 2010.
- [16] J.M. Tang, R. Nabben, C. Vuik, and Y.A. Erlangga. Comparison of two-level preconditioners derived from deflation, domain decomposition and multigrid methods. *Journal of Scientific Computing*, 39:340–370, 2009.
- [17] A. Van der Sluis and H.A. Van der Vorst. The rate of convergence of conjugate gradients. *Numer. Math.*, 48(5):543–560, 1986.
- [18] P. Vaněk, J. Mandel, and M. Brezina. Algebraic multigrid by smoothed aggregation for second and fourth order elliptic problems. *Computing*, 56:179–196, 1996.